INVESTIGATION OF SUPERALLOY COMPOSITION SPACE USING HIGH THROUGHPUT THIN FILM SYNTHESIS AND SYNCHROTRON X-RAY DIFFRACTION

LD Connor[1], PM Mignanelli[2], S Guérin[3], JP Soulié[3], C Mormiche[3], S Frost[3], R Greenhalgh[3], BE Hayden[3], HJ Stone[2]

[1] Diamond Light Source Limited, Harwell Campus, Didcot, OX11 0DE
[2] University of Cambridge, Department of Materials Science and Metallurgy, Cambridge, CB3 0FS
[3] Ilika technologies Ltd, Kenneth Dibben House, Enterprise Road, Southampton, SO16 7NS

Keywords: TCP, High-throughput, Synchrotron, X-ray

Abstract

The development of new nickel-base superalloys, which commonly contain in excess of 10 alloying elements, is a challenge with nearly unparalleled complexity. The vast number of alloying element combinations and the amount of each element that can be added means that the efficient design of new alloys requires the use of computational techniques. However, the viability of the computationally designed alloys is founded upon the fidelity of the databases used to calculate the thermodynamic equilibrium phases.

In this work, high-throughput physical vapour deposition has been used to assess the Ni-Cr-Co and Ni-Cr-W ternary systems. The synthesis of compositionally graded thin film samples has allowed a large area of composition space to be assessed and the use of synchrotron X-ray diffraction to analyse the thin film samples has provided a method of phase identification at a resolution beyond that achievable with laboratory-based techniques. The data acquired has allowed previously unknown phases in these ternary systems to be identified, the extent of the constituent phase fields to be determined and enabled the compositional dependence of the γ lattice parameter to be obtained.

Introduction

New nickel-base superalloys continue to be required to meet the evolving environmental and performance demands of gas turbine engine designs [1,2]. These include both higher performance alloys and those with a balance of properties better tailored to specific applications within the engine. However, the development of new alloys is challenging as, following 50 years of continual innovation, commercially available superalloys possess a good balance of properties for high temperature service [3,4]. It is therefore widely accepted that a computational alloy design framework is desirable over the experimental, trial-and-error approaches that have been used historically. This is believed to be particularly important if new alloys are to be effectively designed and optimised for specific applications within the engine.

The Integrated Computational Materials Engineering (ICME) initiative is seeking to achieve this by establishing a virtual framework for alloy and component design. This initiative offers the potential of reducing alloy development cycles to periods comparable to engine component design cycles, thereby allowing components with optimal performance to be produced [5]. Such computational alloy design approaches have already been successfully used to design new nickel-base superalloys [6,7]. These alloy design tools typically combine empirical and physically based models of the materials properties and how they relate to alloy chemistry within an optimisation loop. One key feature of these models is the need to provide predictions of phase equilibria. Whilst such predictions are, in principle, possible using *ab-initio* computational methods they are limited in the number of atoms that may be simulated, and are therefore restricted to comparatively simple alloy chemistries. This is particularly problematic for nickel-base superalloys, which can include up to 10 different elements at a range of different concentrations. As such, predictions of phase equilibria for computational alloy design typically make use of the CALPHAD (CALculation of PHAse Diagrams) approach, which determines the stable phases by comparing their relative free energies, calculated using thermodynamic parameter databases that have been constructed from experimental data [8]. This approach also offers the advantage that predictions can be made of multi-element systems sufficiently rapidly to allow combinatorial alloy studies or closed-loop compositional optimisation against a set of predetermined targets. Critically, the fidelity with which phase equilibria can be predicted for a given alloy chemistry is dependent on the availability of substantial amounts of high quality experimental data. However, such data is increasingly scarce for ternary and higher order systems. This makes the creation of databases with suitable accuracy particularly challenging as the relative magnitudes of the free energy curves must be self-consistent across all composition space considered if reliable predictions are to be obtained.

High throughput alloy screening techniques offer the potential of evaluating the large ranges of composition space that must be covered to allow the creation of thermodynamic databases with improved accuracy. To be effective, such techniques must combine both high throughput synthesis and characterisation methods. Alloy synthesis can be accomplished by compositionally-graded physical vapour deposition (PVD) or blown-powder/wire-fed selected laser melting (SLM). Characterisation of the alloys produced is necessarily limited to those techniques that are amenable to batch processing rather than individual sample testing. Suitable techniques include X-ray phase identification and spatially resolved compositional mapping, although other tests may be envisaged if suitable automation can be established.

In this work, PVD has been used to create compositionally graded thin film samples from which phase identification has been performed using spatially resolved high-energy synchrotron X-ray diffraction. Attention has focused on characterising selected ternary systems implicated in the formation of undesirable topologically close packed (TCP) phases in superalloys. It is well known that these phases lead to deterioration in alloy properties and, as such, their occurrence must be understood if component lives are to be maximised [9–11]. The experimentally determined phase equilibria have been compared with predictions of the same systems using two commercially available databases and phase

diagrams available in the literature. Comparisons have also been made between data acquired from the thin film samples and from bulk material processed using more conventional fabrication techniques.

Experimental methods

Deposition of compositionally graded thin film samples
Synthesis of the thin film samples was performed at Ilika plc, Southampton, UK using a proprietary High-Throughput PVD system. This system allows the simultaneous co-deposition of up to 6 elements using a shadowing technique that controls the amount of material arriving at a given position on the substrate [12]. A schematic diagram of the PVD source, the substrate, and the adjustable aperture used to achieve the compositionally graded deposition is shown in Figure 1.
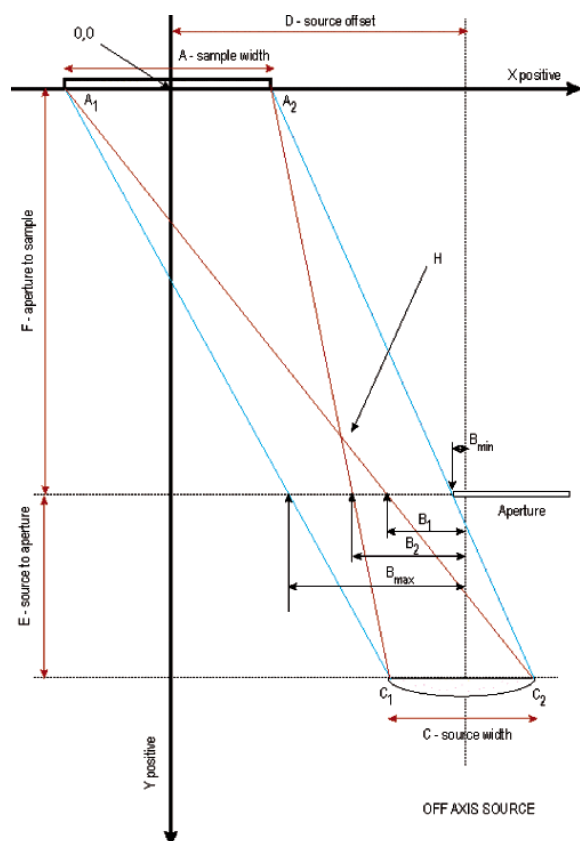

Figure 1. Schematic diagram showing the PVD source and substrate configuration [12].

The constituent elements of the ternary alloys investigated in this study were evaporated from solid material, of purity $\geq$ 99.99%, using Knudsen cells or electron guns, by increasing their temperature to achieve a suitable vapour pressure in the vacuum. Each elemental source was individually controlled to achieve the required evaporation rate and gradient of material across the substrate surface. Since the elements were all deposited at the same time, with no moving parts, intimate mixing was achieved during deposition. This obviated the need for long duration homogenisation heat treatments and eliminated the possibility of forming lower order intermetallic compounds. For all of the systems investigated, the thin films were deposited at room temperature on 35×35 mm^2 quartz substrates and annealed in an

ultra high vacuum at 900 °C for 2 hours to ensure the formation of the thermodynamically stable phases of the systems studied at this temperature. Following annealing, the compositions of the thin films were determined using Energy Dispersive X-ray (EDX) analysis in a 14×14 grid measurements performed with a step size of 1 mm.

Synchrotron X-ray diffraction of thin film samples
X-ray diffraction measurements of phases across the compositionally graded thin film samples were performed using synchrotron radiation at the I12 beamline instrument which is part of the Diamond Light Source, Didcot, UK [13]. A monochromatic beam of 53 keV (0.2339Å) was obtained using a Si {111} bent Laue monochromator and calibrated using a CeO$_2$ standard. The incident beam dimensions of 500×500 µm were defined by a set of Tungsten slits just prior to the thin film sample. Each thin film sample was affixed to an X-Y positioning stage and translated through the incident X-ray beam. The Debye-Scherrer diffraction cones were collected using a 2D Pixium RF4343 area detector positioned approximately 760 mm downstream of the incident synchrotron beam. This geometry allowed acquisition of diffraction data in transmission through both the thin film sample and the quartz substrate. The entire area of the sample was then translated relative to the beam in a step-wise manner to allow the collection of individual diffraction spectra from a 49×49 square grid of measurement points with a step size of 600 µm.

Diffraction Data Refinement Strategy
The two-dimensional diffraction patterns were azimuthally integrated using the software package Nika [14] written as a plugin macro for the data analysis package Wavemetrics Igor Pro (https://www.wavemetrics.com) and using the sample-detector distance, X-ray wavelength and detector orientation angles obtained from the CeO$_2$ calibration. This enabled individual intensity versus 2θ diffraction spectrum to be obtained for each of the 2401 measurement positions. Each diffraction spectrum was reviewed to identify the crystallographic phases present, prior to performing a Pawley refinement using the diffraction data analysis software package *TOPAS* [15], from which the lattice parameters of the constituent phases were obtained. The input file that seeded the *TOPAS* refinement was set up in such a way that a single master file was created and, for each spectrum, the observed crystallographic phases were included or excluded from the refinement depending on their predetermined presence or absence from the spectrum.

Bulk material production and characterisation
To provide a direct comparison between the results obtained from the thin film samples and bulk samples, ingots weighing approximately 50 g were cast of selected alloy compositions by vacuum arc melting using material with purity $\geq$ 99.9%. The material was subsequently encapsulated in glass ampoules back-filled with argon, to reduce oxidation, and homogenised at 1250 °C to reduce solidification-induced microsegregation. These samples were then subjected to long duration thermal exposures of 1000 hours at 900 °C to allow the thermodynamically stable states to be approached. Scanning electron microscopy of the heat-treated samples was performed using a FEI Nova NanoSEM 450 in back scattered electron imaging (BEI) mode and compositional data was acquired using the same instrument with a Bruker XFlash 6 solid-state EDX detector. High resolution synchrotron X-ray powder diffraction data were acquired from the bulk samples using 15 keV (0.2339Å) X-rays and the multi-

analyser crystal (MAC) detector system available on the I11 beamline instrument at the Diamond Light Source, Didcot, UK [16]. Analysis of the diffraction data was performed with the *TOPAS* diffraction data analysis software.

Thermodynamic modelling
Isothermal sections at 900 ˚C of the Ni–Cr–W and Ni–Cr–Co ternary systems were calculated using the Thermocalc software package with both the TCNi7 and TTNi8 databases, supplied by Thermo-Calc Software, AB and Sente Software Ltd respectively. In these simulations, all phases were included.

Results

The 900 ˚C isothermal sections of the Ni-Cr-W ternary system predicted using the Thermo-Calc software with the TCNi7 and TTNi8 databases are shown in Figure 2a and 2b respectively. In these figures, the limits of the predicted single phase field are shown as blue lines, red lines indicate the boundaries of two- and three-phase fields and tie-lines in the two-phase fields are shown in green. Overlaid onto these figures are the experimental data acquired from the diffraction data analysis of the thin film samples. To facilitate visualisation of the various phase fields, the data points have been coloured-coded, as indicated by the legend shown to the right of Figure 2b. In comparing the experimental and predicted data, it can be seen that the experimentally determined γ phase field extends to considerably higher Cr concentrations than is predicted by either TCNi7 or TTNi8 or is represented in the available literature [17, 18].
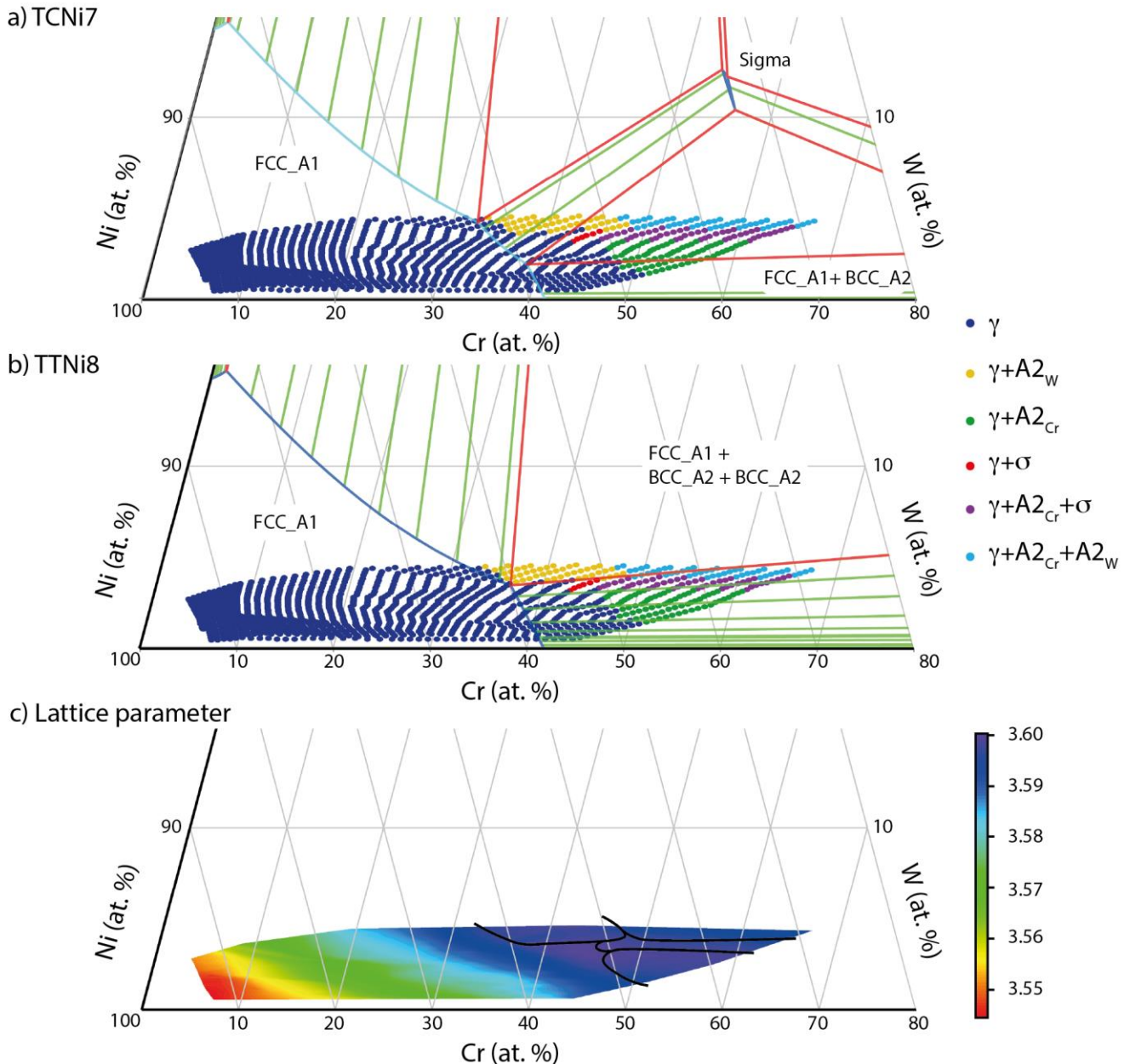

Figure 2. Experimentally determined phase data (data points) of the Ni-Cr-W system at 900 ˚C overlaid on thermodynamic equilibria predicted using Thermo-Calc with the (a) TTNi8 database and (b) TCNi7 database. (c) the measured γ lattice parameter.

One of the most significant differences between the phase equilibria predicted by the two thermodynamic databases is the occurrence of the sigma phase in TCNi7. Whilst a single-phase field for the sigma phase was not identified in the experimental phase appears to exist for significantly lower W concentrations (~ 4 at% W) than that predicted by TCNi7 (~ 10 at% W). However, the TCNi7 database is unable to predict the three-phase $\gamma+A2_{Cr}+A2_{W}$ phase field, which was identified from the experimental data.

The variation in the lattice parameters of the gamma phase across the range of compositions examined is shown in Figure 2c. As expected, the lattice parameter of this phase increases with concentration of both Cr & W, with W leading to a more rapid rise for a give elemental concentration in line with its larger atomic radius.

Using the same approach, the extent of the one, two and three phase fields in the Ni-Cr-Co system, predicted using the TCNi7 and TTNi8 databases, and experimentally determined through synchrotron X-ray diffraction of thin film samples, is shown in Figure 3. Comparison of the experimental and predicted data shows that there is a good correlation between the locations of the predicted and measured boundaries of the gamma phase field with both of the thermodynamic databases. However, the locations of the boundaries with the secondary phases were not in such good agreement.

The experimental data acquired from the Ni-Cr-Co ternary system clearly indicated the presence of two distinct sigma phases, as indicated by the mauve and black data points. These two sigma phases were separately distinguished through the differing intensities of the peaks in their diffraction spectra and their respective compositional ranges over which they were observed.

Examples of the synchrotron X-ray diffraction data obtained from the thin film sample in regions containing the sigma phases are shown in Figure 4. The locations of the measurements are shown in Figure 4a and the azimuthally integrated diffraction data from the points marked by the black cross markers are shown in Figures 4b & 4c. The blue traces in Figure 4b & 4c correspond to the $\gamma+A2_{Cr}$ two-phase field, located towards the bottom of the ternary section. The transition to the $\gamma+\sigma_{NiCr}$ region can be seen in the green diffraction data. The γ then decreases as the σ_{NiCr} becomes a more dominant phase. Finally, the presence of the second σ_{CoCr} becomes apparent in the darker green traces as the Co content increases, after which the data shows spectra consistent with the single phase σ_{CoCr} (red traces).

In addition to revealing the presences of two sigma phases, the experimental data also clearly delineated the two-phase fields ($\gamma+\sigma_{CoCr}$, $\gamma+\sigma_{NiCr}$, $\sigma_{CoCr}+\sigma_{NiCr}$) between the various sigma and gamma phases and the three-phase field ($\gamma+\sigma_{CoCr}+\sigma_{NiCr}$). Importantly, the presence of these two different sigma phases was not predicted by either of the thermodynamic databases, nor are they reported in the available Ni-Cr-Co phase diagrams available in the literature [19–21]. This is perhaps unsurprising given the similarity between the crystal structures and nearly continuous nature of the two individual sigma phase fields, with only a narrow two-phase field between them. Notably, the sigma phase field predicted by TCNi7 and TTNi8 are in good agreement with one another, which is perhaps to be expected given their common origins with previously published phase diagrams. Whilst there

data, a two-phase field between sigma and gamma was observed (red markers) along with a three-phase $\sigma+\gamma+A2_{Cr}$ (purple markers). Notably, the experimentally observed sigma

was also good agreement between the experimental data and the predictions made with TTNi8 database over the concentration of cobalt at which a sigma phase may formed, the experimental results obtained in the present study suggest that the sigma phase field extends to lower Cr contents. The differences in the boundaries of the predicted and experimentally determined sigma phase fields have a concomitant impact on the locations of the surrounding two-and three-phase regions.
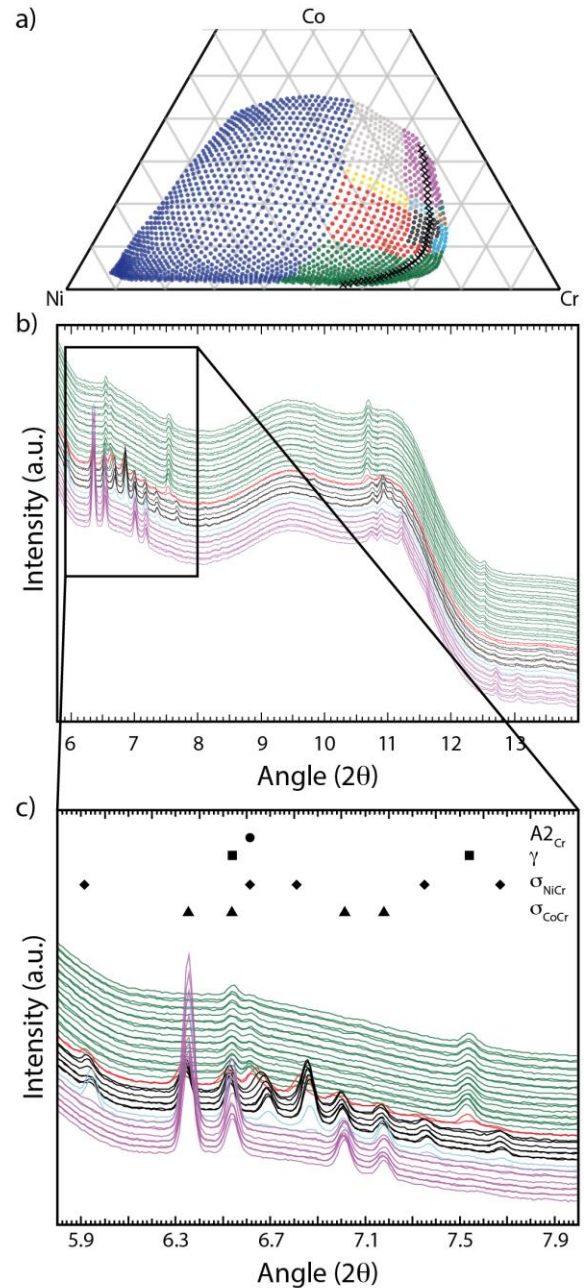

Figure 4. a) Locations of synchrotron X-ray diffraction measurements shown in b) synchrotron X-ray diffraction data of the NiCrCo thin-film and c) the identified phases
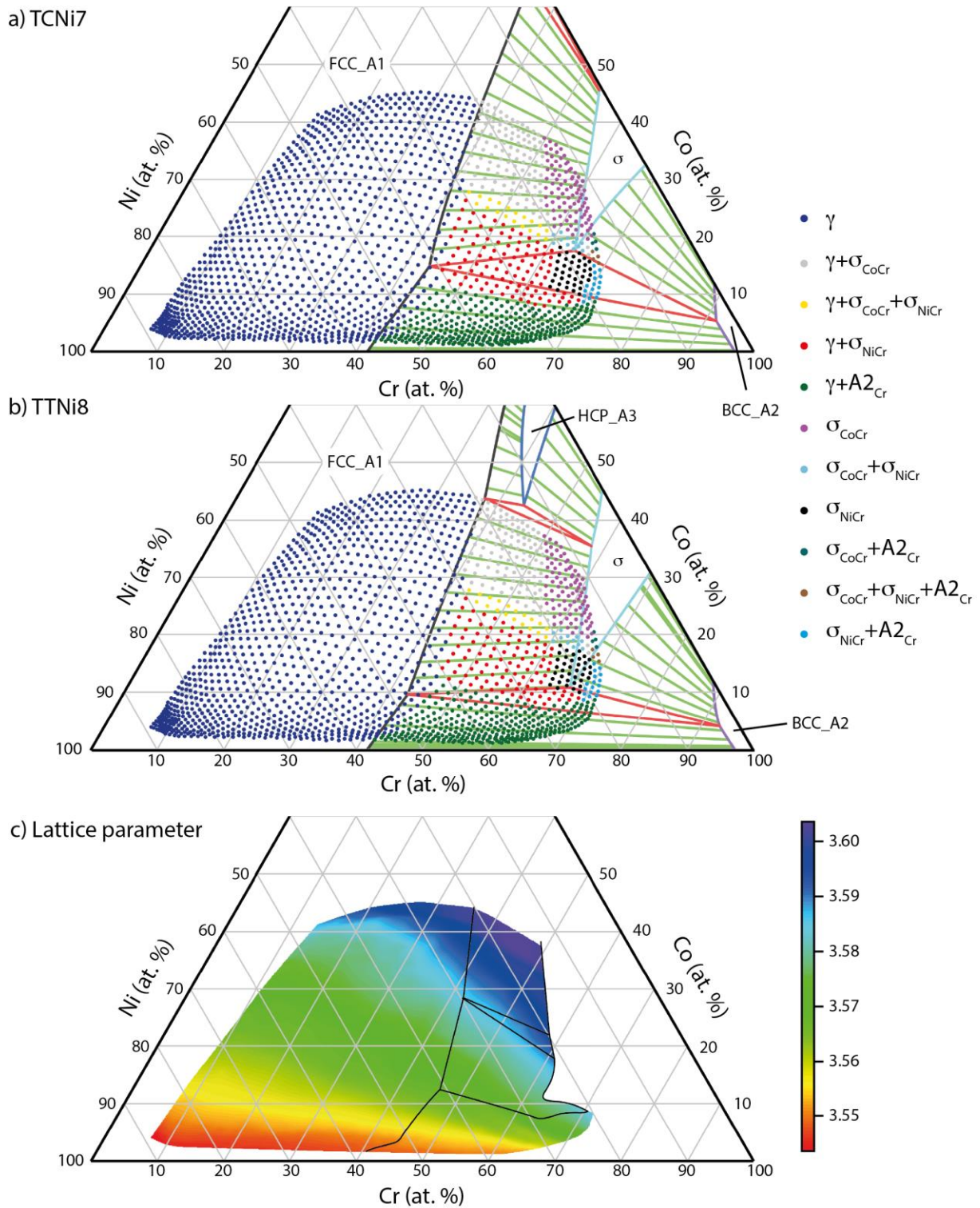
Figure 3. Experimentally determined phase data of the Ni-Cr-Co system at 900˚C overlaid with thermodynamic equilibria, predicted using Thermo-Calc with (a) the TTNi8 database and (b) the TCNi7 database presented alongside (c) the measured γ lattice parameter.

Using the method previously described, the γ lattice parameter was determined for the range of compositions explored, and this is plotted in Figure 3c. This shows smooth colour contours, with the lattice parameter increasing slowly with increased levels of alloying. In addition, the lattice parameter was observed to increase more rapidly with additions of Co than with additions of Cr.

To confirm the presence of the sigma regions identified in the analysis of the thin film samples and facilitate more detailed

characterisation, bulk samples were prepared with compositions of 22Ni-45Cr-30Co at% and 31Ni-52Cr-17Co at%. These compositions were selected as they lie within the two-phase γ+sigma fields.
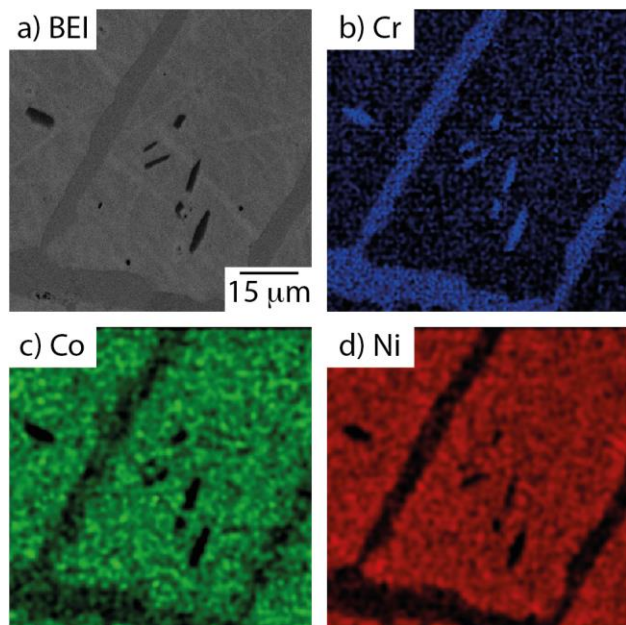

Figure 5. BEI and EDX maps of the bulk 22Ni–45Cr–30Co at% sample after thermal exposure at 900˚C for 1000 hours.
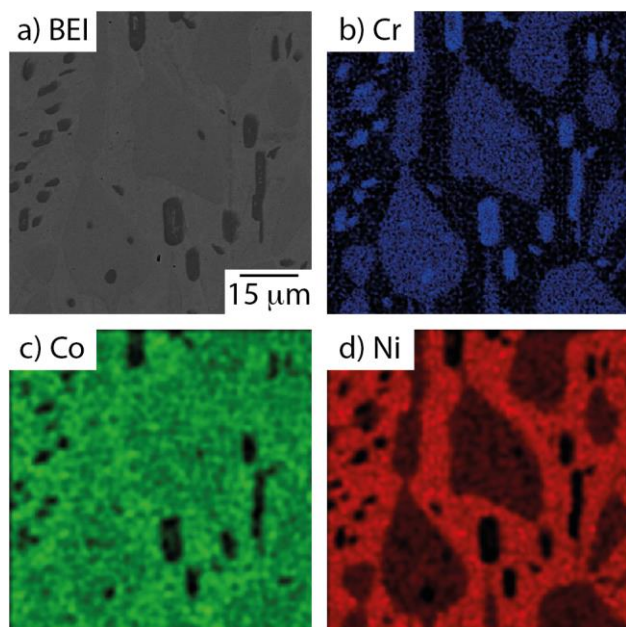

Figure 6. BEI and EDX maps of the bulk 31Ni–52Cr–17Co at% sample after thermal exposure at 900˚C for 1000 hours.

Back-scattered electron images of these two alloys following thermal exposure for 1000 hours at 900 ˚C are shown in Figures 5a and 6a respectively. Both of the microstructures show three distinct phases, as seen from the varying contrast revealed by the BEI. The compositional distribution was measured across the two alloys using EDX analysis and the resultant elemental concentration maps are shown in Figures 5b-d and 6b-d. These data, in conjunction with the BEI, indicate that both microstructures consisted of the expected γ matrix and sigma phases, but also contained A2$_{Cr}$. The A2$_{Cr}$ is not anticipated to be a thermodynamically stable in these alloys, but forms in the early stages of the ageing heat treatment to relieve the chromium supersaturation in the γ matrix from the solution heat treatment prior to the formation of slower growing, thermodynamically stable sigma phase. As such, it is expected that more than 1000 hours of thermal exposure would be required to reach full equilibrium in these alloys.

The compositions of the three phases identified in Figures 5 and 6 were determined using spot EDX analysis and the results are presented in Tables 1 and 2. These data show pronounced differences between the Ni and Co concentrations in the sigma phases. Whilst these observations support the conclusions drawn from the EDX maps, their differing structures cannot be conclusively drawn from these data alone.

Table 1. Compositions of the phases in 22Ni–45Cr–33Co at% after 1000 hours 900˚C, obtained using point-wise EDX analysis.

	Ni	Cr	Co
γ matrix	24.0	39.7	36.3
σ$_{CoCr}$	11.4	61.9	26.7
A2$_{Cr}$	5.4	77.0	17.6

Table 2. Compositions of the phases in 31Ni–52Cr–17Co at% after 1000 hours 900˚C, obtained using point-wise EDX analysis.

	Ni	Cr	Co
γ matrix	36.9	43.8	19.3
σ$_{NiCr}$	19.1	64.0	16.9
A2$_{Cr}$	5.8	87.4	6.8

To confirm that the two sigma phases observed in the bulk samples were distinct phases, high resolution synchrotron X-ray powder diffraction was performed on these samples. The diffraction patterns obtained from these samples are presented in Figure 7. Whilst the two diffraction patterns clearly show the presence of reflections consistent with the presence of a sigma phase, their relative intensities differ. These patterns are consistent with those acquired from the thin film samples, shown in Figure 4, albeit fewer reflections were observed in the thin film data owing to inferior counting statistics of all the reflections acquired.

Discussion

The comparison of the data acquired from the thin film samples with the thermodynamic predictions using the two commercially available databases revealed disparities between all three datasets. The TCNi7 and TTNi8 databases both showed good cross-correlation in the prediction of the γ phase field. This was also in agreement with the experimental observations of the extent of the γ phase field in the Ni–Cr–Co system, although higher concentrations of W were observed to be accommodated in this phase in the experimental data acquired from the Ni–Cr–W system than was predicted with either of the two databases. However, the disparities between the experimental data and the thermodynamic predictions were more pronounced with the phase fields of the secondary phases.
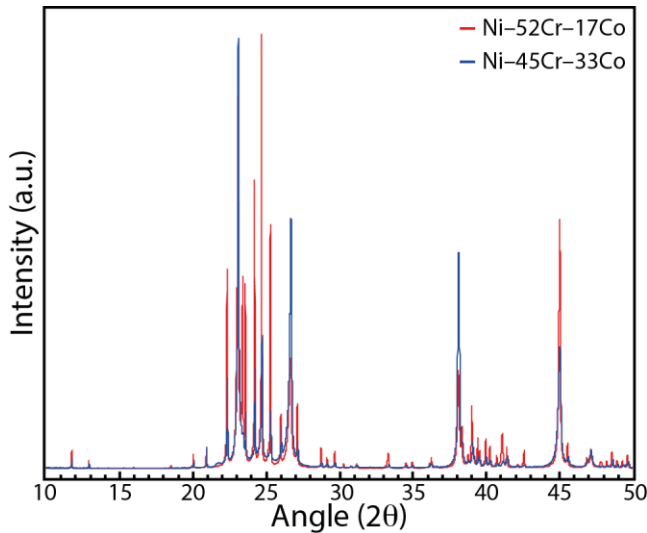
Figure 7. High resolution synchrotron X-ray powder diffraction data was acquired from the Ni–52Cr–17Co and Ni–45Cr–33Co at% samples.

In the Ni–Cr–W system, the experimental data confirmed the presence of a sigma phase, in agreement with the predictions of TCNi7 database, although its location differed considerably. Similarly, differences were observed between the sigma phase in the Ni–Cr–Co. Most notably the experimental data acquired from the thin film samples suggested that two distinct sigma phases may actually exist and these results were supported by observations made on bulk samples. Differences were also observed between the locations of the predicted and measured phase boundaries. For any extra credence to be given to the experimental data over that predicted with thermodynamic modeling, it is necessary to examine the factors that influence the reliability of the experimental results.

Central to the efficacy of the thin film technique for the high throughput sampling of composition space are: ensuring that the equilibria are established in the thin film samples; and, the thin films may be reliably characterised. These issues are discussed separately below.

Equilibrium was achieved in the thin film samples through a heat treatment of 2 hours at 900˚C. An estimate of the diffusion distance of any elemental species can be made using the equation, $x=\sqrt{(Dt)}$, where x is the distance, D is the diffusion coefficient and t is the time. Calculation of the diffusion distance for W, the slowest diffusing element investigated here, using a diffusion coefficient available in the literature [22], revealed a diffusion distance of ~0.33 μm. In comparison, the average thickness of the thin film was measured to be less than 500 nm. This would therefore allow for diffusion from the surface through two thirds of the sample, before any additional benefits from the increased velocity of surface diffusion are considered.

The acquisition of spatially resolved composition data over the necessary length scales is routine and reliable. In contrast, the analysis of the diffraction data acquired from the thin film presents a number of challenges. Preliminary investigations using a range of different substrate materials identified that the thin film diffraction signal may be obscured by that of the substrate upon which it is deposited. However, even with an appropriate amorphous substrate, characterisation of the reflections from the thin films remained difficult due to their intrinsically low signal to noise ratio. This made it difficult to unambiguously determine the phases present, whilst local texture prohibited structural refinement. To aid in the analysis of the thin film diffraction data, diffraction patterns obtained from bulk samples in one and two-phase regions proved invaluable. This approach was found to be most effective when performed in a feedback loop, whereby areas of interest or of high complexity identified during the analysis of the thin film material were selected for the preparation of bulk samples. Higher quality diffraction data acquired from these bulk samples could then be used to aid analysis of the thin film diffraction data from within these regions and obtain improved confidence in the results obtained.

These issues potentially impact the ease with which these techniques may be extended to other ternary and high order systems appropriate to superalloys. Specifically, the difficulty in identifying minority diffraction peaks would present particular challenges for the characterisation of systems containing the γ and γ′ phases as their crystallographic similarity and the low intensity of the superlattice reflections may prohibit effective discrimination of these phases. This would also have a commensurate impact upon the ability to obtain reliable lattice parameter data for γ+γ′ alloys. Whilst it has been shown here that the lattice parameter of the γ phase may be readily obtained from analysis of diffraction data from alloys where the γ reflections may be isolated, accurate fitting of the γ′ reflections in γ+γ′ alloys would be harder and more complex. This would also directly impact on any calculations of the lattice misfit, which are so critical to the design of polycrystalline and single crystal nickel-base superalloys.

In summary, the results of this research have shown that thin film PVD offers a method for the high-throughput analysis of superalloy composition space. Furthermore, when coupled with high-resolution synchrotron X-ray diffraction, highly detailed phase identification data can be performed. This combination of techniques has the potential to both screen composition space for the development of new superalloys and provide vast amounts of detailed phase equilibria data that can be incorporated into the thermodynamic databases, improving the quality of their predictions.

Conclusions

Simultaneous elemental deposition using a vapour-shadowing technique allowed the creation of thin film samples from the Ni–Cr–W and Ni–Cr–Co ternary systems. Spatially resolved compositional analysis and synchrotron diffraction enabled characterisation of the phases present, from which sections of the respective ternary phase diagrams were obtained. Key observations from the data acquired include; the observation of a sigma phase in the Ni–Cr–W system, and the identification of two distinct sigma phases in the Ni–Cr–Co system. Comparisons made with thermodynamic models using commercially available databases identified discrepancies between the predictions made and the experimental data. The results obtained through this work provide rich datasets of the phase equilibria in these two ternary systems that underlie superalloy composition space. Such data may be used to improve the fidelity with which predictions may be made using Thermodynamic models, thereby allowing more

reliable design of new superalloys. The ability to obtain the γ lattice parameter, using synchrotron X-ray diffraction has also been demonstrated, allowing the compositional variation of this property to be better understood and potentially incorporated into models of lattice misfit.

References

1. European aeronautics: A vision for 2020, European Commission, 2001.

2. Flightpath 2050 Europe's vision for aviation, European Commission, 2011.

3. C.T. Sims, "A history of superalloy metallurgy for superalloy metallurgists," *Superalloys*, 1984, 399–419.

4. R.F. Decker, "The evolution of wrought age-hardenable superalloys," *The Journal of The Minerals, Metals & Materials Society*, 58 (9) (2006) 32–36.

5. J. Allison, D. Backman and L. Christodolou, "Integrated Computational Materials Engineering: A new paradigm for the global materials profession," *The Journal of The Minerals, Metals & Materials Society*, vol. 58 (11) (2006), 25–27.

6. G.B. Olson, "Computational design of hierarchically structured materials," *Science*, 277 (1997), 1237-1242.

7. R.C. Reed, T. Tao and N. Warnken, "Alloys-by-design: Application to nickel-based single crystal superalloys," *Acta Materialia*, 57 (2009), 5898-5913.

8. U.R. Kattner, "The Thermodynamic modelling of multicomponent phase equilibria," *The Journal of The Minerals, Metals & Materials Society*, 49 (12) (1997), 14–19.

9. R.L. Dreshfield R.L. Ashbrook, "Sigma phase formation and its effect on stress-rupture properties of IN-100," (NASA Technical note D-5185, 1969).

10. X.Z. Qin et al., "Long-term thermal exposure responses of the microstructure and properties of a cast Ni-base superalloy," *Materials Science and Engineering A*, 543 (2012), 121–128.

11. N.G. Jones et al., "Influence of elevated Co and Ti levels on polycrystalline powder processed Ni-base superalloy," *Materials Science and Technology*, 30 (2014), 1853–1861.

12. S. Guerin and B.E. Hayden, "Physical Vapor Deposition Method for the High-Throughput Synthesis of Solid-State Material Libraries," *Journal of Combinatorial Chemistry*, 8 (2006), 66-73.

13. M. Drakopoulos et al., "I12: the Joint Engineering, Environment and Processing (JEEP) beamline at Diamond Light Source," *Journal of Synchrotron Radiation*, 22 (2015), 828-838.

14. J. Ilavsky, "Nika - software for 2D data reduction," *Journal of Applied Crystallography*, 45 (2012), 324-328.

15. A.A. Coelho, TOPAS. Version 4.0, Bruker AXS GmbH, Karlsruhe, Germany, 2008.

16. S.P. Thompson et al., "Beamline I11 at Diamond: a new instrument for high resolution powder diffraction", *Review of Scientific Instruments*, 80 (2009), 075107.

17. K.P. Gupta, "The Cr-Ni-W (chromium-nickel-tungsten) system," *Phase diagrams ternary nickel alloys*, 1 (1990), 111–133.

18. P. Gustafson, "A thermodynamic evaluation of the Cr-Ni-W system", *CALPHAD: Comput. Coupling Phase Diagrams Thermochem*, 12 (1988), 277–292.

19. T. Chart, A. Dinsdale and F. Putland, "The NPL ALLOYDATA Bank: Its Use in the Calculation of Phase Diagrams for Super-Alloy Development," *Special Publication-Chemical Society*, 1980, 234–245.

20. L.Kaufman and H. Nesor, "Calculation of superalloy phase diagrams: Part I", *Metallurgical Transactions*, 5 (1974), 1617–1621.

21. M.R. Jackson and J.R. Rairden, "Protective coatings for superalloys and the use of phase diagrams" *NBS Spec. Publ.*, 496 (1978), 423–439.

22. M.S.A. Karunaratne and R.C. Reed, "Interdiffusion of the platinum-group metals in nickel at elevated temperatures," *Acta Materialia*, 51 (2003), 2905–2919.